scientific reports

Check for updates

OPEN

Use of shear wave velocity for assessing engineering properties of compacted bentonite after swelling

Mintae Kim[1], Changho Lee[2], Jang-Un Kim[3] & Hyunwook Choo[3]✉

The characteristics of compacted bentonite after swelling determine the long-term stability of barrier systems. Due to the fact that the current stress level is the most important variable in determining the performance of engineered geosystems, this study aims to investigate the stress states and the consequent change in engineering properties of compacted bentonites after swelling. A series of vertical and horizontal swelling pressure tests were performed for compacted bentonites with varying initial dry unit weights at varying pore fluid concentrations. The compacted bentonite samples after swelling were loaded to investigate the changes in lateral stress and deformability. In addition, the shear wave velocity was continuously measured during and after swelling processes. The results of this study demonstrate that the swelling pressure increased with increasing dry unit weight of tested materials and decreasing pore fluid concentrations. The changes in lateral stress and void ratio of compacted bentonite after swelling were only measurable when the applied vertical stress was greater than the swelling pressure, reflecting that the swelling pressure cancels out the externally applied stress. Most notably, this study reveals that the initiation and termination of the swelling process and the change in engineering properties of compacted bentonite after swelling can be determined by measuring shear wave velocity.

Compacted bentonites have been considered as engineering materials for barriers in the deep geological repositories of radioactive waste or for landfill liners because of their characteristics of high swelling potential and swelling pressure[1]. Owing to the complexity of the behavior of compacted bentonite, its swelling characteristics have been extensively studied over several decades to elucidate the effects of mineralogy and microstructure of bentonite, initial water content, dry unit weight, type and concentration of infiltration solution, and temperature on swelling pressure or swelling strain[2–18].

Previous studies have been conducted on the swelling behavior of compacted bentonite while the compacted bentonite expands; however, studies on the behavior of compacted bentonite after swelling are very limited. As the deep geological repositories for high-level nuclear waste or municipal solid waste landfill liners are designed and constructed for long-term operation, studies on the characteristics of the compacted bentonite after swelling must be conducted to ensure the stability of barrier systems. Because the performance of engineered geosystems is primarily determined by the current stress level, the determination of the lateral stress or coefficient of lateral stress at rest (K_0) is critical[19]. However, the determination of in-situ stress levels from traditional geotechnical experiments is challenging because of the difficulty in accessing deep geological repositories or landfill liners. Therefore, non-destructive testing methods would be ideal for investigating the characteristics of compacted bentonite after swelling.

The measurement of the shear wave velocity (V_s) provides informative geophysical characteristics of soils; therefore, many studies have been conducted to explore the application of V_s to the assessment of engineering properties of soils[20–26]. In particular, V_s is determined by the mean effective stress, leading to the measurement of V_s giving an indication of stress levels of in-situ soils. Furthermore, the V_s is dependent on the interaction between soil particles, leading to the fact that the swelling process may be monitored by the continuous measurement of V_s.

[1]School of Civil, Environmental and Architectural Engineering, Korea University, Seoul 02841, South Korea. [2]Department of Civil Engineering, Chonnam National University, Gwangju 61186, South Korea. [3]Department of Civil and Environmental Engineering, Hanyang University, Seoul 04763, South Korea. ✉email: choohw@hanyang.ac.kr

Therefore, in this study, the characteristics of compacted bentonite were experimentally investigated during and after swelling using V_s. The compacted bentonite specimens with varying dry unit weights were prepared under varying NaCl pore fluid concentrations. Vertical and horizontal swelling pressure tests were performed separately during swelling, and V_s was continuously measured. After the completion of swelling, the sample was loaded to examine the variations of the deformation, lateral stress, and V_s of the compacted bentonite after swelling. Considering the complexity of the characteristics of the compacted bentonite, these test results can provide valuable insights into understanding the characteristics of compacted bentonite during and after swelling using the measurement of V_s.

Experimental program

Vertical and horizontal swelling pressure tests at constant volume were performed for compacted bentonite with varying NaCl pore fluid concentrations and dry unit weights. Bender element tests were also executed for the measurement of shear wave velocity to investigate the characteristics of compacted bentonite during and after swelling. Table 1 indicates the experimental program performed in this study.

Test soil and sample preparation. The test soil used in this study is commercially available high plastic clay (USCS group symbol: CH) with a specific gravity (G_s) of 2.51. The liquid limit (LL) and plastic limit (PL) were 89.25% and 38.12%, respectively. Table 2 summarizes the index properties of the tested soil. Based on semi-quantitative analysis (Bruker-Diffrac.EVA) of XRD results, the main mineral type was determined to be montmorillonite, and other mineral types are also reported in Table 2. The ratio between exchangeable Na^+ and Ca^{2+} was 0.34, determined by ICP-OES (Varian 720-ES), indicating that the bentonite employed in this study was Ca-bentonite. Ca-bentonite is a representative bentonite distributed in Korea; thus the selection of Ca-bentonite reflected the regional characteristics.

Type	Dry unit weight (kN/m³)	NaCl concentration (mol/L)			
		0 M	0.1 M	0.5 M	1.0 M
Vertical swelling test	11.77	- Measure the vertical swelling pressure of compacted bentonite during swelling at constant volume			
	12.75				
	13.73				
Thin wall oedometer test	11.77	- Measure the horizontal swelling pressure and shear wave velocity of compacted bentonite during swelling at constant volume - Measure the horizontal stress change and shear wave velcotiy of compacted bentonite after swelling			
	12.75				
	13.73				

Table 1. Experimental program.

Soil type	Calcium bentonite
Specific gravity (G_s)	2.51
Liquid limit, LL (%)	89.24
Plastic limit, PL (%)	38.12
Specific surface area (m^2/g)*	260.56
Cation exchange capacity, CEC (meq/100 g)	90.1
Exchangeable cations (meq/100 g)	Na = 19
	Ca = 56.4
	Mg = 10.2
	K = 4.5
Maximum dry density, MDD (kN/m³)	11.72[a]/14.23[b]
Optimum moisture content, OMC (%)	39[a]/27[b]
Unified soil classification system	High plastic clay
Main minerals (%)	M = 61
	Q = 25
	C = 10
	B = 2

Table 2. Index properties of test soil. *M* montmorillonite, *Q* quartz, *B* biotite, *C* calcite. [a]Standard A compaction test, [b]modified compaction test, *methylene blue adsorption[24].

For the preparation of soil samples, oven-dried bentonite was poured into a consolidation mold and directly compacted to achieve initial dry unit weights of 11.77, 12.75, and 13.73 kN/m^3 with an initial moisture content of 5%. Note these three different target unit weights were determined based on both standard and modified compaction tests. After completing the compaction of the soil sample, the soil sample was moved into a base container and saturated with NaCl solutions with molar concentrations of 0 (i.e. DI water), 0.1, 0.5, and 1.0 M.

Test procedures during swelling. During the expansion of compacted bentonite, vertical and horizontal swelling pressure tests were performed separately. Figure 1a shows the experimental setup of the vertical swelling pressure test. After the completion of the sample preparation for the vertical swelling pressure test (sample dimension: diameter of 50 mm and height of 20 mm), the vertical swelling pressure generated in the process of pore water infiltration into the sample was directly measured by a load cell.

The horizontal swelling pressure tests were conducted with a customized thin-wall oedometer cell instead of a conventional oedometer cell (Fig. 1b). The thin-wall oedometer cell was made of stainless steel, which has an inner diameter of 50 mm and a wall thickness of 1 mm. The maximum horizontal stress that can be applied to the employed thin-wall oedometer cell is 400 kPa to ensure the K_0 condition (i.e. lateral strain < $5{\cdot}10^{-5}$)[27]. Two strain gauges were symmetrically installed on the outside of the thin-wall oedometer cell at the middle-height of the soil sample (15 mm) to measure the horizontal swelling pressure, and two dummy gauges were also employed for temperature compensation. Before performing the horizontal swelling pressure test, the strain gauges were calibrated using a balloon filled with water to obtain the correlation between the horizontal stress and output voltage (see details in[19]. The soil sample for the horizontal swelling pressure test was prepared using the same procedures as those for the vertical swelling pressure test (sample dimension: diameter of 50 mm and

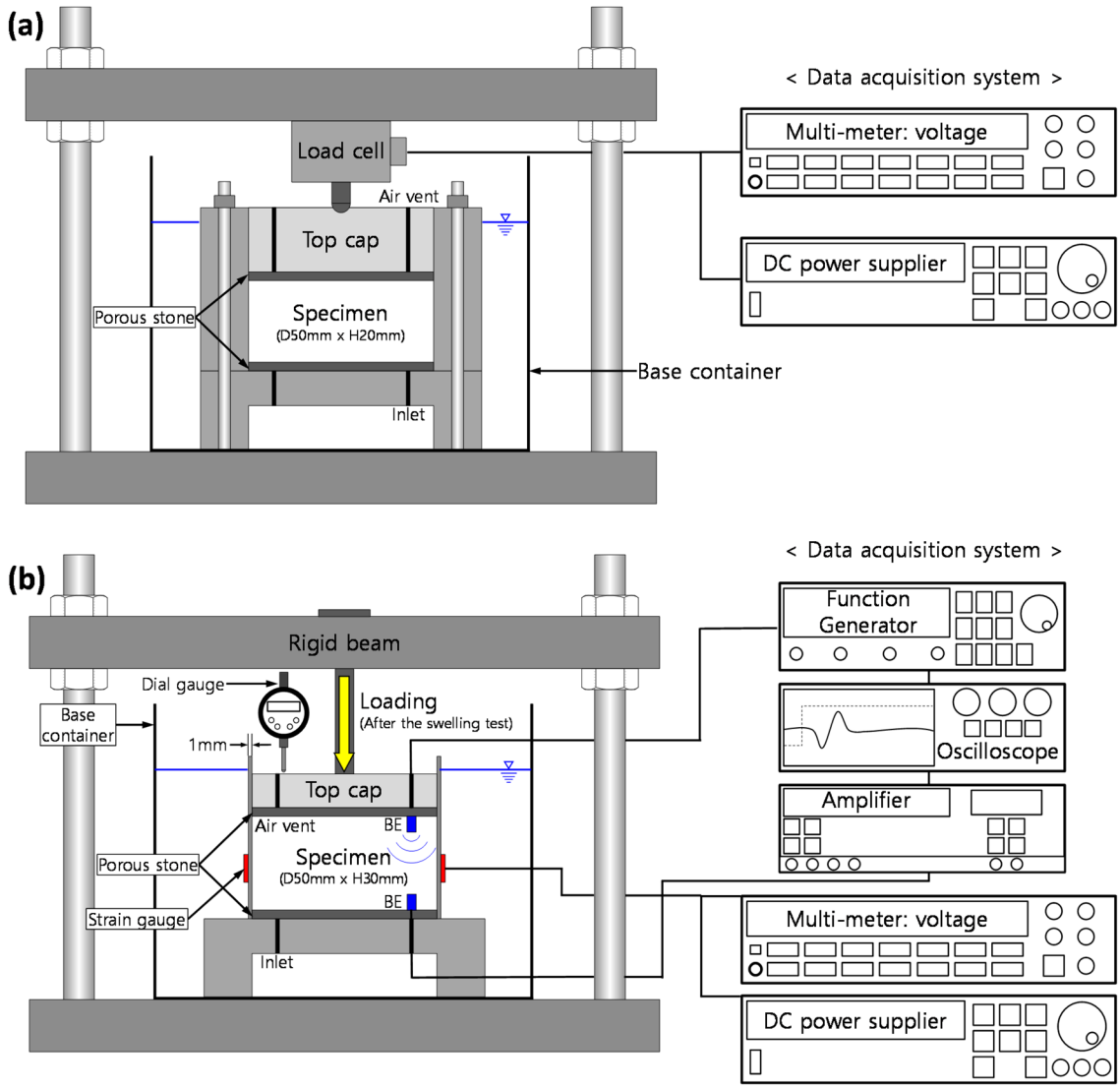

Figure 1. Experimental setup of: (**a**) vertical swelling pressure test and (**b**) horizontal swelling pressure test (loading test after swelling). *BE* bender elements.

height of 30 mm). During both the vertical and horizontal swelling pressure tests, the volume of the sample was constantly maintained.

For the measurement of shear wave velocity, the bender elements (source and receiver elements) were installed at the bottom of the thin-wall oedometer cell and at the top cap (Fig. 1b). The square wave with frequency = 20 HZ and amplitude = 10 V, generated by a function generator (Agilent, 34970A), propagated through the specimen. The received signal was filtered and amplified by a filter amplifier (Krohn-Hite, 3364), and the filtered and amplified signal was digitized by an oscilloscope (Agilent, 54624A). To eliminate random noise, 1024 received signals were averaged. The tip-to-tip distance between bender elements was used as the travel distance, and the first arrival time was chosen from the recorded data in consideration of the near-field effect (see details in[28]. The shear wave velocity was continuously measured until the swelling was completed.

Test procedures after swelling. After completing the horizontal swelling test with the thin-wall oedometer cell, the soil sample was loaded to investigate the characteristics of compacted bentonite after swelling. The vertical stress was gradually loaded up to 297 kPa and the horizontal stress was measured by using strain gauges, as mentioned earlier. Each loading step lasted for 24 h and the shear wave velocity was obtained at the end of each loading step. In addition, the deformation of the soil sample during the loading tests was measured using a digital dial gauge attached to the top cap, and subsequently, the void ratio was calculated to investigate the deformation characteristics of compacted bentonite after swelling.

Results and discussion

Measurements during swelling. *Vertical and horizontal swelling pressures.* Figure 2a–c show the variations in the vertical and horizontal swelling pressures (σ'_{sw}) of compacted bentonite with increasing time during swelling at a constant volume with varying NaCl concentrations for initial dry unit weights of 11.77, 12.75, and 13.73 kN/m^3, respectively. During the swelling process, a significant increase in σ'_{sw} was observed with increasing time at the earlier stage of tests. Then, the rate of change in σ'_{sw} gradually decreased, and ultimately the σ'_{sw} reached a constant value.

As the initial dry unit weight of the soil sample increased, the measured σ'_{sw} increased for all NaCl concentrations (Fig. 2). An increase in the dry unit weight indicates an increase in the quantity of montmorillonite (i.e. swelling clay mineral) at a given volume and the consequent decrease in the distance between swelling particles; therefore, the measured σ'_{sw} increased with increasing dry unit weight[10,15,16,29–33]. As the NaCl concentration increased, the σ'_{sw} decreased (Fig. 2). An increase in NaCl concentration results in a decrease in the double layer thickness, which in turn causes σ'_{sw} to decrease[7–9,17,30,34,35].

Figure 2 also demonstrates that the measured swelling pressure of tested compacted bentonite with higher pore fluid concentrations approached an asymptotic point at an earlier time during the test than that with lower concentrations (see the arrows in Fig. 2). Because the double layer thickness reduces with increasing NaCl concentrations, it can be postulated that the tested compacted bentonite with a high pore fluid concentration has a shorter water flow path between the inside and outside of the diffuse double layer. Additionally, the hydraulic conductivity increases with increasing pore fluid concentrations[36]. Thus, the swelling process can be ceased at a relatively earlier time for tested bentonite with high pore fluid concentrations.

The vertical and horizontal swelling pressures (σ'_{sw}) of tested bentonites were determined as the final value of the swelling process shown in Fig. 2. The determined vertical and horizontal σ'_{sw} are summarized in Table 3. Overall, the vertical σ'_{sw} was higher than the horizontal σ'_{sw} measured at a constant volume in this study. The determined ratio between the horizontal σ'_{sw} and vertical σ'_{sw} ranges from 0.836 to 0.977 (average ratio = 0.890 with a coefficient of variation = 4.62%). This anisotropic swelling pressure can be attributed to the anisotropic microstructure of compacted bentonite, and the determined swelling pressure ratio is comparable with the reported values of previous studies[37].

Shear wave velocity. Figure 3 shows the measured shear wave velocity (V_s) of the tested compacted bentonites with varying pore fluid concentrations and dry unit weights during swelling. Notably, the shear wave velocity of compacted bentonite was measured using the bender element test during the measurement of horizontal swelling pressures under a constant volume (Fig. 1b). As shown in Fig. 3, the measured V_s gradually decreased with time and reached a constant value. With an increase in initial dry unit weight, the measured V_s increased at a given time; however, the effect of pore fluid concentration on the variation of V_s was insignificant (Fig. 3).

The V_s of soils is determined by interparticle contact stiffness and interparticle coordination[24,38–40]. Because an increase in applied stress results in an increase in the interparticle contact area and a consequent increase in contact stiffness between particles, V_s of dry or saturated soils can be expressed as the power function of applied vertical stress (σ'_v):

$$V_s = \alpha \cdot \left(\frac{\sigma'_v}{1kPa}\right)^{\beta}, \tag{1}$$

where α and β are the fitting parameters. α reflects the material constant, strongly influenced by interparticle coordination (or packing state), and β indicates the sensitivity of tested materials on applied stress. In the case of unsaturated soils, the matric suction (u_a–u_w, where u_a = pore air pressure and u_w = pore water pressure) gives an additional increase in interparticle contact stiffness[41]. Thus, Eq. (1) can be modified as[42]:

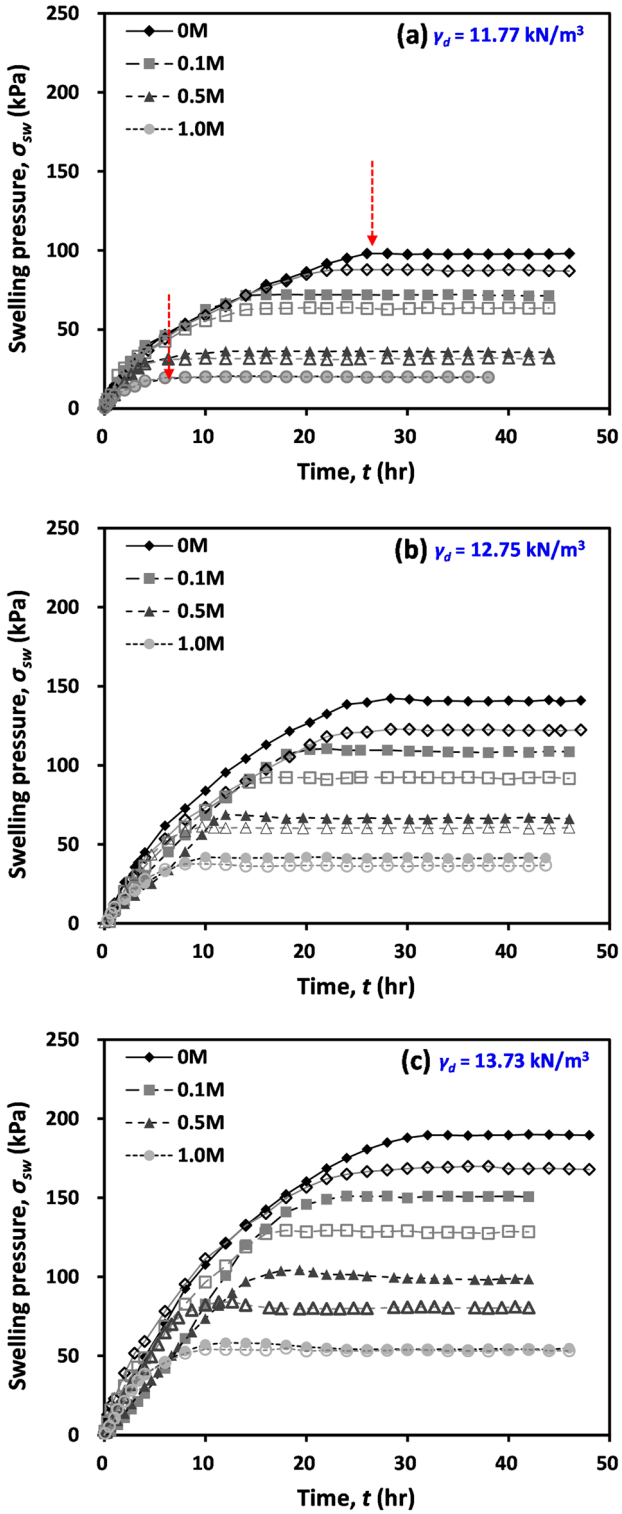

Figure 2. Evolution of vertical and horizontal swelling pressures with respect to time for varying NaCl concentrations: (**a**) specimens with initial dry unit weight $\gamma_d = 11.77$ kN/m^3; (**b**) $\gamma_d = 12.75$ kN/m^3; and (**c**) $\gamma_d = 13.73$ kN/m^3. In the figure, the vertical swelling pressures are presented by filled symbols, and hollow symbols indicate the horizontal swelling pressures.

Dry unit weight (kN/m^3)	Initial moisture content (%)	NaCl concentration (M)	Swelling pressure (kPa)	
			Vertical swelling pressure	Horizontal swelling pressure
11.77	5	0.0	98.13	87.87
		0.1	72.11	63.99
		0.5	36.4	31.99
		1.0	20.58	20.1
12.75	5	0.0	142.34	122.82
		0.1	110.53	92.48
		0.5	68.86	61.24
		1.0	41.98	38.7
13.73	5	0.0	189.91	169.82
		0.1	151.03	129.39
		0.5	100.53	84.21
		1.0	58.3	54.79

Table 3. Summary of the final vertical and horizontal swelling pressures.

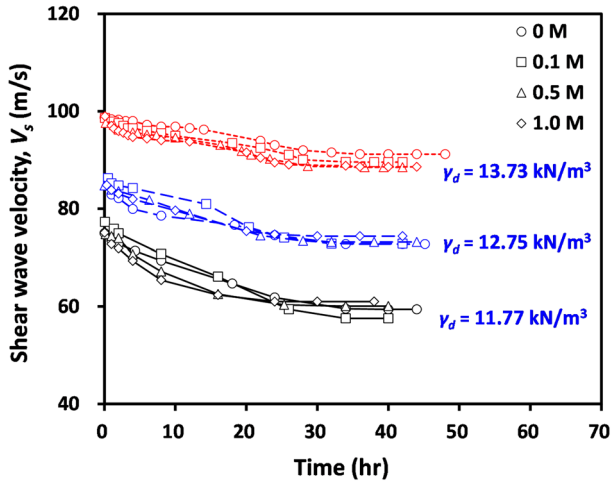

Figure 3. Variation of shear wave velocity of tested compacted bentonites with varying initial dry unit weights and pore fluid concentrations during swelling as a function of time.

$$V_s = \alpha \cdot \left(\frac{\sigma'_v}{1kPa}\right)^{\beta} + \lambda \cdot (u_a - u_w), \tag{2}$$

where λ is the fitting parameter, reflecting the packing state and soil type. The vertical stress was not applied during the swelling process in this study; thus, σ'_v in Eq. (2) can be assumed to be 1 kPa (i.e. top cap weight). Consequently, the V_s of tested compacted bentonite during swelling becomes:

$$V_s \approx \alpha + \lambda \cdot (u_a - u_w). \tag{3}$$

Previous studies[42–44] clearly demonstrated that the magnitude of matric suction decreases with an increase in the degree of saturation, though this study did not measure the matric suction of tested materials. Therefore, the matric suction in Eqs. (2) or (3) decreases according to swelling process. Furthermore, the generation of swelling pressure results in an increase in the spacing between clay particles[45]. This indicates a decrease in interparticle coordination during swelling and a consequent decrease in α in Eqs. (2) or (3). Thus, the measured V_s during swelling decreased with time (Fig. 3).

It is known that a decrease in void ratio (or increase in mass density) results in an increase in matric suction[42]. In addition, the initial packing state of tested soils directly determines the magnitude of α in Eq. (3). Therefore, the measured V_s at a given time increases with an increasing initial dry unit weight of tested soils (Fig. 3).

Time-dependent variations in both swelling pressure and shear wave velocity appear to be closely related (Figs. 2 and 3). Thus, the rate of changes in the swelling pressures ($d\sigma'_{sw}/dt$, where σ'_{sw} = swelling pressure and t = time) and shear wave velocity (dV_s/dt) at a dry unit weight = 11.77 kN/m^3 and NaCl concentration = 0 M was plotted as a function of time, as shown in Fig. 4. It can be observed in Fig. 4 that the rate of change in V_s resembles

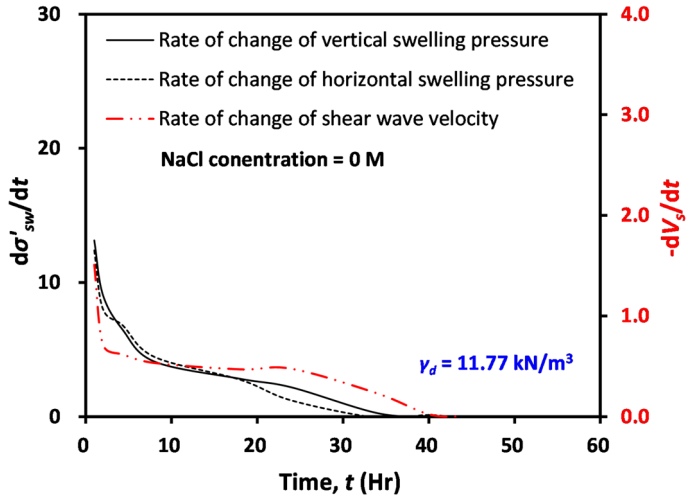

Figure 4. The rate of change in swelling pressure and that in shear wave velocity of tested materials with initial dry unit weight = 11.77 kN/m^3 and NaCl concentration = 0 M according to time.

that in σ'_{sw}, reflecting that the swelling process or the generation of σ'_{sw} causes a decrease in V_s. In addition, it can be inferred from similar time-dependent behaviors between swelling pressure and shear wave velocity that the measurement of shear wave velocity can be used to determine the initiation and termination of a swelling process.

Measurements during loading (after swelling). *Deformation of compacted bentonite.* To determine the deformation characteristics of compacted bentonite after the swelling process, the change in void ratio of soil samples was determined as a function of the applied vertical stress, as shown in Fig. 5. Figure 5 clearly demonstrates that the measured void ratio of all tested materials was constant up to certain points of stress levels despite the increasing applied vertical stress. As the applied vertical stress further increased, the void ratio of tested materials started to decrease. The determined applied vertical stress when the void ratio started to decrease (i.e. yield stress σ'_y) of tested materials is compared with swelling pressure in Fig. 6. Note that the swelling pressure (σ'_{sw}) in Fig. 6 is the average of vertical and horizontal swelling pressures reported in Table 3. Most notably, Fig. 6 indicates that the σ'_y of the tested sample with initial unit weight (γ_d) = 11.77 kN/m^3 coincides with the σ'_{sw} in Table 3. By contrast, the σ'_y of tested samples with initial γ_d = 12.75 and 13.73 kN/m^3 deviates from the σ'_{sw}.

Because of the sample preparation method employed in this study, the tested compacted bentonite experiences compaction-induced yield stress (or preconsolidation stress). In the case of tested specimens with initial γ_d = 11.77 kN/m^3, the target density can be easily achieved by applying relatively low compaction energy. Thus, in the case of tested materials with γ_d = 11.77 kN/m^3, the determined σ'_{sw} was greater than that of compaction-induced σ'_y. Consequently, the σ'_{sw} may act as a preconsolidation stress for the sample with initial γ_d = 11.77 kN/m^3, causing the compacted bentonite after swelling to show negligible settlement until the applied vertical

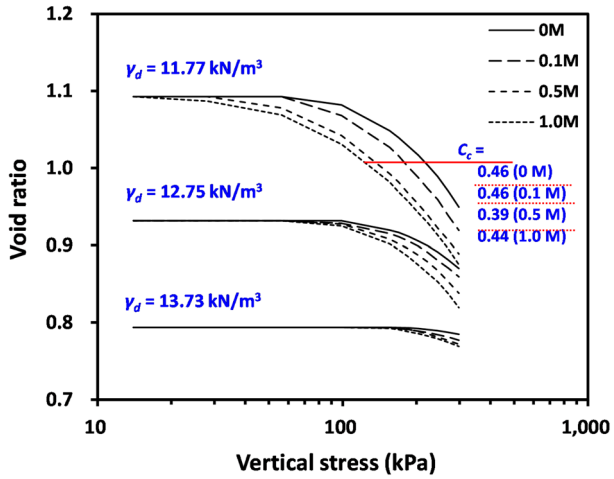

Figure 5. Variation of void ratios of compacted bentonite samples after swelling according to applied vertical stress. C_c compression index.

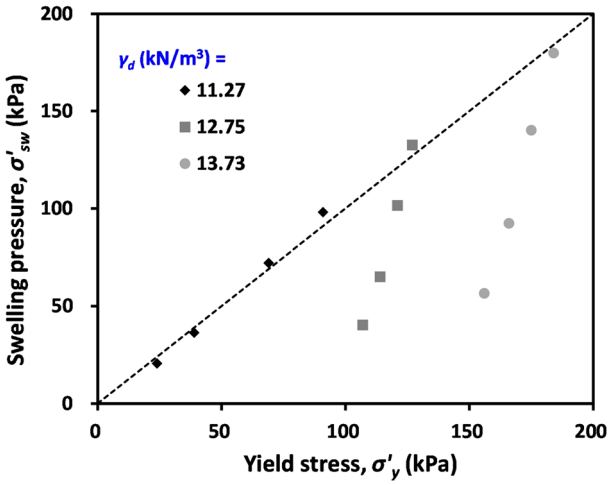

Figure 6. Comparison between swelling pressure and yield stress.

effective stress is greater than σ'_{sw}. By contrast, the tested specimens with a higher target density required higher compaction energy. Thus, it can be postulated that the compaction-induced σ'_y was greater than σ'_{sw} in the case of tested materials with initial $\gamma_d = 12.75$ and 13.73 kN/m^3. Relatively narrow variations of σ'_y with varying NaCl concentrations and σ'_y always being greater than σ'_{sw} support this explanation (Figs. 5 and 6).

The mechanical properties of tested materials with initial $\gamma_d = 12.75$ and 13.73 kN/m^3 involved the impact of compaction-induced yield stress. Thus, to emphasize the sole impact of swelling pressure on the engineering properties of compacted bentonite after swelling, the following sections report the changes in compressibility, lateral stress, and shear wave velocity of compacted bentonite with initial $\gamma_d = 11.77$ kN/m^3 after swelling.

The deformation of soils is the result of a change in effective stress. Thus, it can be assumed that the clay particles in the compacted bentonite after swelling do not experience any increase in effective stress until the initiation of deformation because the internal swelling pressure cancels out the external stress. Consequently, the external stress (or applied vertical effective stress, σ'_v) exceeding the swelling pressure (σ'_{sw}) will cause an increase in effective stress of clay particles, leading to the deformation (void ratio change, Δe) of compacted bentonite after swelling in Fig. 5 can be expressed as:

$$\Delta e = C_c \cdot log\left(\frac{\sigma'_v}{\sigma'_{sw}}\right), \text{when } \sigma'_v > \sigma'_{sw} \tag{4}$$

where C_c denotes the compression index. Note, Eq. (4) is identical to the inverse of the equation for calculating heave from the constant swell test[46]. The determined C_c values are given in Fig. 5, and the C_c values for tested materials with initial $\gamma_d = 11.77$ kN/m^3 are comparable to those in the authors' previous study on saturated bentonite with similar void ratio[47], reflecting that the deformation characteristics of compacted bentonite after swelling may be similar to those of saturated bentonite without swelling.

Figure 5 also demonstrates the effect of NaCl concentrations on the compressibility of tested compacted bentonite after swelling: the void ratio at a given applied stress level decreases with increasing NaCl concentration. Because swelling pressure (or σ'_y) decreases with increasing NaCl concentrations (Figs. 2 and 5), the specimen with higher pore fluid concentration can start to deform at lower stress levels, leading to a greater change in the void ratio according to Eq. (4). By contrast, the impact of pore fluid concentration on C_c values was insignificant (Fig. 5).

Applied vertical stress and measured horizontal stress. Figure 7 presents the variation in the measured horizontal stress with increasing applied vertical stress for tested compacted bentonite with initial $\gamma_d = 11.77$ kN/m^3 after swelling. It can be observed in Fig. 7 that, despite the increase in vertical stress on the sample, the horizontal stress remained unchanged up to certain points of stress levels. After passing certain stress levels, the horizontal stress started to increase, and Fig. 7 clearly indicates that the stress level for the initiation of lateral stress increases coincides with the swelling pressure. This observation reconfirms that the swelling pressure cancels out the externally applied stress; thus, the change in lateral stress was only measurable when the applied vertical stress was greater than swelling pressure.

From the change in measured horizontal stress ($\Delta\sigma'_h$) and that in applied vertical stress ($\Delta\sigma'_v$), the coefficient of lateral earth stress at-rest (K_0) was calculated according to (triangle in Fig. 7):

$$K_0 = \frac{\Delta\sigma'_h}{\Delta\sigma'_v}, \text{when } \sigma'_v > \sigma'_{sw} \tag{5}$$

The determined K_0 is given in Fig. 7, and it can be observed in Fig. 7 that the effect of pore fluid concentration on the determined K_0 was insignificant. Thus, high lateral stress at a given applied vertical stress with increasing NaCl concentration can be attributed to the small swelling pressure with increasing pore fluid concentration.

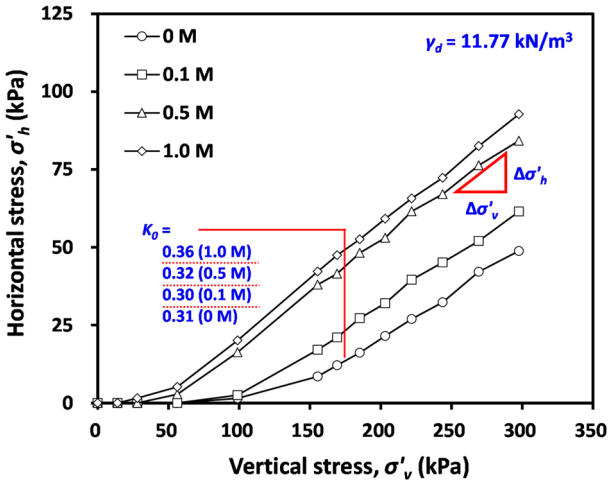

Figure 7. Variation in the measured horizontal stress with increasing applied vertical stress for tested compacted bentonite with initial $\gamma_d = 11.77$ kN/m^3 after swelling.

K_0 of saturated clay generally ranges from 0.5 to 1, which is greater than the determined K_0 of tested materials after swelling. It is known that the wetting of compacted bentonite with inundation may not ensure the fully saturated condition of compacted bentonite[48],thus, the tested compacted bentonite after swelling may contain some portion of matric suction. Note that the K_0 of unsaturated clay based on elasticity theory can be expressed as a function of matric suction (u_a–u_w)[49] as follows:

$$K_0 = \frac{\mu}{1-\mu} - \frac{1-2\mu}{1-\mu} \cdot \frac{X \cdot (u_a - u_w)}{(\sigma_v - u_a)}, \tag{6}$$

where X = fitting parameter, ranging from 0 to 1. Thus, with an increase in matric suction (or with a decrease in the degree of saturation), the K_0 decreases according to Eq. (6), leading to the measured K_0 of tested compacted bentonite after swelling (Fig. 7) being smaller than the typical K_0 of saturated clay.

Shear wave velocity (V_s). Figure 8a shows the measured shear wave velocity (V_s) of compacted bentonite with initial $\gamma_d = 11.77$ kN/m^3 according to applied vertical stress. Exhibiting similarity to the results of deformation (Fig. 5) and lateral stress (Fig. 7), V_s did not increase until the applied vertical effective stress (σ'_v) approached the swelling pressure (σ'_{sw}), reflecting a negligible change in interparticle contact stiffness when σ'_v was smaller than σ'_{sw}. Figure 9 shows the measured shear waves with loading steps for compacted bentonite with initial dry unit weight (γ_d) = 11.77 kN/m^3 and NaCl concentration = 0 M. Figure 9 also clearly indicates that the change in first arrival time (dotted circle in Fig. 9) was only measurable when the σ'_v approached σ'_{sw}. When σ'_v exceeded σ'_{sw}, V_s increased with increasing applied vertical stress. Thus, the V_s of tested materials after swelling can be expressed as:

$$V_s = \alpha' \cdot \left(\frac{\sigma'_v - \sigma'_{sw}}{1kPa} \right)^{\beta}. \tag{7}$$

Figure 8b shows the variation of V_s as a function of (σ'_v–σ'_{sw}) (Eq. (7)). Tested compacted bentonite after swelling shows very comparable V_s at a given (σ'_v–σ'_{sw}) regardless of pore fluid concentrations, reflecting that a higher V_s at a given applied stress with increasing NaCl concentration in Fig. 8a can be attributed to the earlier initiation of V_s increase with increasing pore fluid concentration resulting from a smaller swelling pressure. The typical stress exponent β of dry or saturated soils is approximately 0.25. However, the determined β of tested compacted bentonite after swelling is approximately 0.1, implying that the measured V_s after swelling still includes the contribution from the matric suction (Eq. (2)). Thus, this smaller β of tested compacted bentonite after swelling compared to typical dry or saturated soils reinforces that the tested material is not fully saturated after swelling.

In summary, in the case where the applied vertical stress (σ'_v) is smaller than swelling pressure (σ'_{sw}), the change in the internal effective stress of soils is minimal (Fig. 7). Therefore, the tested compacted bentonite after swelling shows a negligible change in compressibility and shear wave velocity when σ'_v is smaller than σ'_{sw}. When there is a change in internal effective stress (i.e. $\sigma'_v > \sigma'_{sw}$), the tested soils show a change in mechanical properties. This in turn demonstrates that the continuous measurement of shear wave velocity can provide insight into the change in internal effective stress of compacted bentonite after swelling. Thus, the change in engineering properties of compacted bentonite after swelling can be determined through the measurement of shear wave velocity.

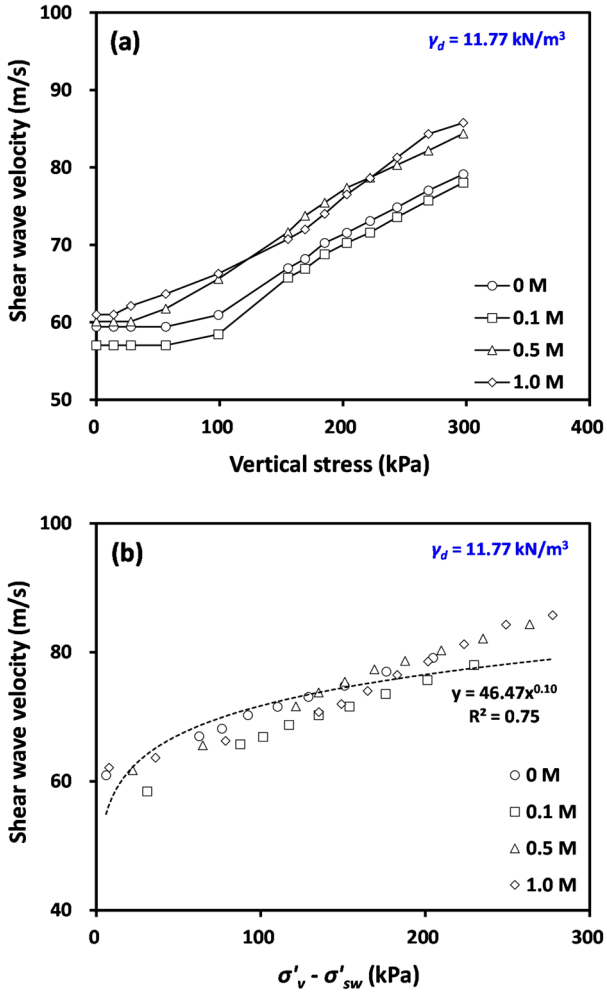

Figure 8. Variations of shear wave velocity of tested compacted bentonite after swelling according to (**a**) applied vertical stress and (**b**) difference between applied vertical stress and swelling pressure.

Conclusion

This study experimentally investigated the characteristics of compacted bentonite during and after swelling using the measurement of shear wave velocity (V_s). The compacted bentonite specimens with varying dry unit weights were prepared under varying NaCl pore fluid concentrations. The vertical and horizontal swelling pressures and V_s of tested compacted bentonite were measured during the swelling process at a constant volume. In addition, the soil sample was loaded to investigate the variations of the deformation, lateral stress, and V_s of the compacted bentonite after swelling. The key findings of this study are as follows:

(1) The swelling pressure (σ'_{sw}) increased with increasing dry unit weight of tested materials because of an increase in the quantity of swelling clay mineral at a given volume. In addition, the σ'_{sw} increased with decreasing pore fluid concentrations because of an increase in double layer thickness.
(2) Time-dependent variation of V_s resembles that of σ'_{sw}, reflecting that the measurement of shear wave velocity can be used to determine the initiation and termination of a swelling process.
(3) The changes in lateral stress and void ratio of compacted bentonite after swelling were only measurable when the applied vertical stress was greater than the swelling pressure, reflecting that the swelling pressure cancels out the externally applied stress.
(4) Because V_s is mainly determined by interparticle stiffness, which is the function of the internal effective stress of soils, the measurement of V_s can capture the change in engineering properties of compacted bentonite after swelling.

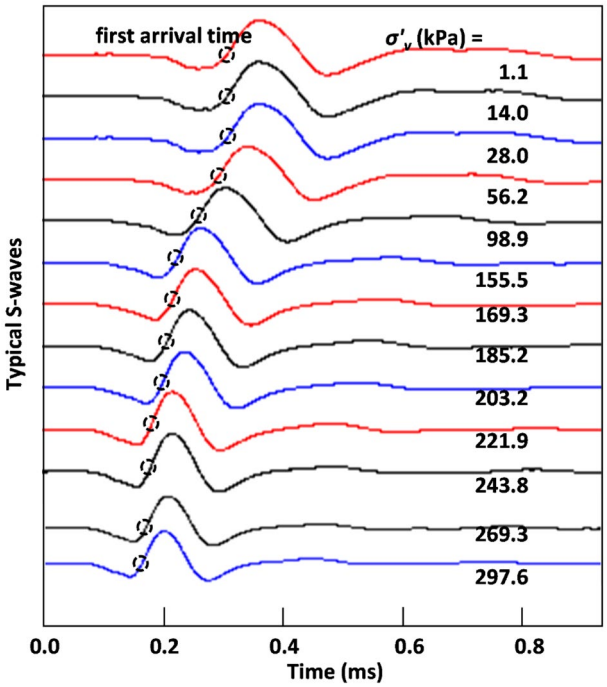

Figure 9. Measured shear waves with loading for compacted bentonite with initial dry unit weight = 11.77 kN/m^3 and NaCl concentration = 0 M after swelling.

Data availability

All data generated or analyzed during this study are available from the corresponding author on reasonable request.

Received: 24 May 2023; Accepted: 14 September 2023
Published online: 21 September 2023

References

1. Zhang, F. & Cui, Y. J. Microstructure-based insight into different swelling pressure determination methods. *Eng. Geol.* **307**, 106777 (2022).
2. Basmas, A. A., Al-Homoud, A. S. & Husein, A. Laboratory assessment of swelling pressure of expansive soils. *Appl. Clay Sci.* **9**(5), 355–368 (1995).
3. Bian, X., Cui, Y. J. & Li, X. Z. Void effect on the swelling behaviour of compacted bentonite. *Géotechnique* **69**(7), 593–605 (2019).
4. Bradbury, M. H. & Baeyens, B. Porewater chemistry in compacted re-saturated MX-80 bentonite. *J. Contam. Hydrol.* **61**, 329–338 (2003).
5. Dąbska, A. & Léthel, A. Swelling behaviours of compacted lime-softening sludge for application in landfill liners. *Sci. Rep.* **11**(1), 1–13 (2021).
6. Geneste, Ph., Raynal, M., Atabek, R., Dardaine, M. & Oliver, J. Characteristics of a French clay barrier and outline of the experimental programme. *Eng. Geol.* **28**, 443–454 (1990).
7. Jadda, K. & Bag, R. Variation of swelling pressure, consolidation characteristics and hydraulic conductivity of two Indian bentonite due to electrolyte concentration. *Eng. Geol.* **272**, 105637 (2020).
8. Karnland, O. *Bentonite Swelling Pressure in Strong NaCl Solutions—Correlation Between Model Calculations and Experimentally Determined Data. SKB Technical Report 98–01* (Swedish Nuclear Fuel and Waste Management Co., 1998).
9. Katsumi, T., Ishimori, H., Onikata, M. & Fukugawa, R. Long-term barrier performance of modified bentonite materials against sodium and calcium permeant solutions. *Geotext. Geomembr.* **26**(1), 14–30 (2008).
10. Komine, H. & Ogata, N. Experimental study on swelling characteristics of compacted bentonite. *Can. Geotech. J.* **31**, 478–490 (1994).
11. Mekonnen, E., Amdie, Y., Etefa, H., Tefera, N. & Tafesse, M. Stabilization of expansive black cotton soil using bioenzymes produced by ureolytic bacteria. *Int. J. Geo-Eng.* **13**(1), 10 (2022).
12. Pusch, R. Mineral-water interactions and their influence on the physical behavior of highly compacted Na bentonite. *Can. Geotech. J.* **19**(3), 381–387 (1982).
13. Shehata, A., Fall, M., Detellier, C. & Alzamel, M. Effect of groundwater chemistry and temperature on swelling and microstructural properties of sand–bentonite for barriers of radioactive waste repositories. *Bull. Eng. Geol. Environ.* **80**(2), 1857–1873 (2021).
14. Villar, M. V., Gómez-Espina, R. & Gutiérrz-Nebot, L. Basal spacings of smectite in compacted bentonite. *Appl. Clay Sci.* **65–66**, 95–105 (2012).
15. Villar, M. V. & Lloret, A. Influence of dry density and water content on the swelling of a compacted bentonite. *Appl. Clay Sci.* **39**, 38–49 (2008).
16. Wang, Q., Cui, Y., Tang, A. M., Li, X. & Ye, W. Time- and density-dependent microstructure features of compacted bentonite. *Soils Found.* **54**(4), 657–666 (2014).
17. Ye, W. M. *et al.* Influence of salt solutions on the swelling behavior of the compacted GMZ01 bentonite. *Environ. Earth Sci.* **74**(1), 793–802 (2015).

18. Zhang, C. L. & Kröhn, K. P. Sealing behaviour of crushed claystone–bentonite mixtures. *Geomech. Energy Environ.* **17**, 90–105 (2019).
19. Shin, H. & Santamarina, J. C. Mineral dissolution and the evolution of k_0. *J. Geotech. Geoenviron. Eng.* **135**(8), 1141–1147 (2009).
20. Chang, I. & Cho, G. A new alternative for estimation of geotechnical engineering parameters in reclaimed clays by using shear wave velocity. *Geotech. Test. J.* **33**(3), 171–182 (2010).
21. Fayed, A. L. & Mouda, A. A. Shear wave velocity in the East Nile Delta Clay: Correlations with static CPT measurements. *Geotech. Geol. Eng.* **38**, 2303–2315 (2020).
22. Oh, T., Band, E., Cho, G. & Park, E. Estimation of undrained shear strength for saturated clay using shear wave velocity. *Mar. Georesour. Geotechnol.* **35**(2), 236–244 (2017).
23. Roesler, S. K. Anisotropic shear modulus due to stress anisotropy. *J. Geotech. Eng. Div.* **105**(7), 871–880 (1979).
24. Santamarina, J. C., Klein, K. A. & Fam, M. A. *Soils and Wave-Particular Materials Behavior, Characterization and Process Monitoring* (Wiley, 2001).
25. Sully, J. P. & Campanella, R. G. Evaluation of in-situ anisotropy from crosshole and downhole shear wave velocity measurements. *Géotechnique* **45**(2), 267–282 (1995).
26. Yan, L. & Byrne, P. M. Simulation of downhole and crosshole seismic test on sand using the hydraulic gradient similitude method. *Can. Geotech. J.* **7**(4), 441–460 (1990).
27. Okochi, Y. & Tatsuoka, F. Some factors affecting K_0-values of sand measured in triaxial cell. *Soils Found.* **24**(3), 52–68 (1984).
28. Lee, J. S. & Santamarina, J. C. Bender elements: performance and signal interpretation. *J. Geotech. Geoenviron. Eng.* **131**(9), 1063–1070 (2005).
29. Komine, H. Simplified evaluation for swelling characteristics of bentonites. *Eng. Geol.* **71**, 265–279 (2004).
30. Lee, J., Lim, J., Kang, I. & Kwon, S. Swelling pressures of compacted Ca-bentonite. *Eng. Geol.* **129–130**, 20–26 (2012).
31. Schanz, T. & Al-Badran, Y. Swelling pressure characteristics of compacted Chinese Gaomiaozi bentonite GMZ01. *Soils Found.* **54**(4), 748–759 (2014).
32. Tripathy, S., Sridharan, A. & Schanz, T. Swelling pressure of compacted bentonites from diffuse double layer theory. *Can. Geotech. J.* **41**, 437–450 (2004).
33. Wang, Q., Tang, A. M., Cui, Y., Delage, P. & Gatmiri, B. Experimental study on the swelling behaviour of bentonite/claystone mixture. *Eng. Geol.* **124**, 59–66 (2012).
34. Komine, H., Yahuhara, K. & Murakami, S. Swelling characteristics of bentonites in artificial seawater. *Can. Geotech. J.* **46**, 177–189 (2009).
35. Motoshima, T., Iso, S. & Nishimura, T. Behavior of compacted Ca-bentonite subjected to HMC loading observations and interpretation. *MATEC Web Conf. EDP Sci.* **27**, 04004 (2021).
36. Won, J., Kim, J. U. & Choo, H. Estimation of the swelling strain and swelling pressure of compacted bentonite using electrical conductivity. *Appl. Clay Sci.* **242**, 107040 (2023).
37. Saba, S., Barnichon, J. D., Cui, Y. J., Tang, A. M. & Delage, P. Microstructure and anisotropic swelling behaviour of compacted bentonite/sand mixture. *J. Rock Mech. Geotech. Eng.* **6**(2), 126–132 (2014).
38. Choo, H. & Lee, C. Inverse effect of packing density on shear wave velocity of binary mixed soils with varying size ratios. *J. Appl. Geophys.* **194**, 104457 (2021).
39. Choo, H., Nam, H. & Lee, W. A practical method for estimating maximum shear modulus of cemented sands using unconfined compressive strength. *J. Appl. Geophys.* **147**, 102–108 (2017).
40. Mitchell, J. K. & Soga, K. *Fundamentals of Soil Behavior* Vol. 3 (Wiley, 2005).
41. Sadeghabadi, A., Noorzad, A. & Zad, A. Numerical and experimental modeling of geomechanical behavior of partially saturated soils. *Int. J. Geo-Eng.* **12**, 1–22 (2021).
42. Clariá, J. J. & Rinaldi, V. A. Shear wave velocity of a compacted clayey silt. *Geotech. Test. J.* **30**(5), 399–408 (2007).
43. Cho, G. C. & Santamarina, J. C. Unsaturated particulate materials—Particle-level studies. *J. Geotech. Geoenviron. Eng.* **127**(1), 84–96 (2001).
44. Dong, Y. & Lu, N. Dependencies of shear wave velocity and shear modulus of soil on saturation. *J. Eng. Mech.* **142**(11), 04016083 (2016).
45. Tripathy, S., Bag, R. & Thomas, H. R. Effects of post-compaction residual lateral stress and electrolyte concentration on swelling pressures of a compacted bentonite. *Geotech. Geol. Eng.* **32**(4), 749–763 (2014).
46. Nelson, J. D., Chao, K. C., Overton, D. D. & Nelson, E. J. *Foundation Engineering for Expansive Soils* (Wiley, 2015).
47. Choo, H., Choi, Y., Kim, Y. U., Lee, W. & Lee, C. Compressibility and hydraulic conductivity of calcium bentonite treated with pH-responsive polymer. *Geomech. Eng.* **22**(4), 329–337 (2020).
48. ASTM. *Standard Test Methods for One-Dimensional Swell or Settlement Potential of Cohesive Soils. ASTM D4546–14* (ASTM International, 2014).
49. Lu, N. & Likos, W. J. *Unsaturated Soil Mechanics* (Wiley, 2004).

Acknowledgements

This research was supported by the National Research Foundation of Korea (NRF) grant funded by the Korean government (RS-2023-00221719).

Author contributions

M.K.: Writing, Visualization; C.L.: Conceptualization, Formal analysis; J.-U.K.: Investigation, Methodology; H.C.: Writing & Editing, Supervision, Visualization, Funding acquisition.

Funding

Funding sources are stated in the Acknowledgements.

Competing interests

The authors declare no competing interests.

Additional information

Correspondence and requests for materials should be addressed to H.C.